Coexistence of Bulk Superconductivity and Charge Density Wave in Cu_xZrTe_3

Xiangde Zhu,* Hechang Lei, and C. Petrovic

Condensed Matter Physics and Materials Science Department, Brookhaven National Laboratory, Upton, New York 11973, USA

(Received 17 March 2011; published 15 June 2011)

We report the coexistence of bulk superconductivity with $T_c = 3.8$ K and charge density wave (CDW) in Cu intercalated quasi-two-dimensional crystals of $ZrTe_3$. The Cu intercalation results in the expansion of the unit cell orthogonal to the Zr-Zr metal chains and partial filling of CDW energy gap. We present anisotropic parameters of the superconducting state. We also show that the contribution of CDW to the scattering mechanism is anisotropic in the $\hat{a}$-$\hat{b}$ plane. The dominant scattering mechanism in the normal state for both $ZrTe_3$ and $Cu_{0.05}ZrTe_3$ along the $\hat{b}$ axis is the electron–electron umklapp scattering.

DOI: 10.1103/PhysRevLett.106.246404 PACS numbers: 71.45.Lr, 74.25.F−, 74.70.Xa

Peierls distortion results in the periodic modulation of electron density in solids and generates an energy band gap at the Fermi surface [1]. It can be observed as a charge density wave (CDW) superstructure in many low dimensional materials [2]. The continuous suppression of CDW order brings about superconductivity (SC) in Cu_xTiSe_2 [3]. This is reminiscent of SC in heavy fermion and the cuprate oxide phase diagram when the magnetic order is tuned by pressure (P) or doping to $T \rightarrow 0$ [4–6]. The superconducting mechanism in such electronic systems is likely to be mediated by the magnetic fluctuations [7,8]. Similarly, the domelike structure of $T_c(x)$ and the pairing mechanism in Cu_xTiSe_2 is argued to stem from the type of quantum criticality related to fluctuations in CDW order [9]. Quantum phase transition is proposed to drive CDW order into a quantum nematic phase [10]. On the other hand, the positive slope of the dome could be explained via the shift of the Fermi level caused by Cu intercalation and the negative slope by the enhanced scattering for the high Cu concentration [11]. This is also supported by the evidence for a single gap s-wave order parameter, implying conventional mechanism despite the domelike evolution of $T_c(x)$ [12]. However, a domelike structure of $T_c(P)$ was also discovered using P as a tuning parameter and suggesting that impurity effects may not be responsible for the dome closure [13].

Chalcogenide superconductors represent a weak coupling side of the smectic order, akin to stripe order in cuprates [10]. There is mounting evidence that in such systems CDW states transform into Fermi liquid through an intermediate phase [14]. Therefore it is of interest to study the melting of CDW order parameter and possible nematic phases in a superconductor with a highly related and tunable two-dimensional electronic system.

$NbSe_3$, exhibits two CDW transitions at 145 and 59 K, and becomes a superconductor under pressure [15]. Another trichalcogenide, $ZrTe_3$, accommodates a layered structure, where the metal-metal distances are 0.39, 0.58, and 0.71 nm along the $\hat{a}$, $\hat{b}$, and $\hat{c}$ axis, respectively [16]. The shortest Zr-Zr distances define two sets of chains along the crystallographic $\hat{b}$ axis [Fig. 1(a)]. This results in a Peierls instability and a CDW transition at $T_{CDW} \sim 63$ K with a $\vec{q} \equiv (\frac{1}{14}, 0, \frac{1}{3})$ [17,18]. As opposed to the poor conductivity values of $TiSe_2$ [3], resistivity values of $ZrTe_3$ are up to 2 orders of magnitude smaller and quasi–two dimensional ($\rho_a \sim \rho_b \sim \rho_c/10$) [17]. The $\rho(T)$ is strongly affected by CDW along the crystallographic directions perpendicular to the $\hat{b}$ axis [17]. A giant Kohn anomaly associated with a soft phonon mode and a two-dimensional order parameter has been identified, as well as CDW fluctuations (pseudogap) that extend well above 100 K [19–21]. The CDW vector $\vec{q}$ agrees with the nesting vector from the calculated Fermi surface [16,22]. This is in contrast to chiral CDW [23] in $TiSe_2$ and semimetallic or semiconducting ground state with no signature of CDW

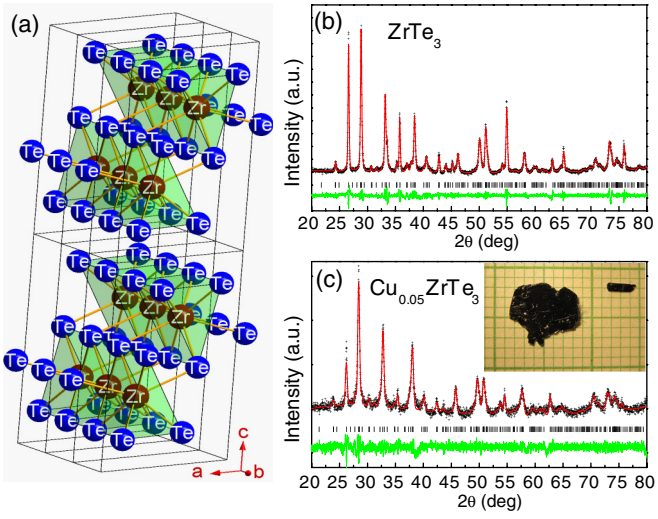

FIG. 1 (color online). (a) The crystal structure of $ZrTe_3$. Crystallographic $\hat{b}$ axis runs along the shortest Zr-Zr distances and the $\hat{c}$ axis is along the vertical. Comparison of the observed (crosses) and calculated (solid line) powder x-ray patterns of $ZrTe_3$ (b) and $Cu_{0.05}ZrTe_3$ (c). The bars (black) correspond to the Bragg reflections and the lowest solid line is the difference between the observed and the calculated patterns.

fluctuation above T_{CDW} [24–26]. The Fermi surface of $ZrTe_3$ contains one quasi-one-dimensional electron like the sheet (pocket) of states of $5p$ Te chain origin that is responsible for CDW distortion and pseudogap formation at $T \gg T_{CDW}$ [16,22]. There is in addition a more isotropic hole sheet that makes up to 90% of the Fermi surface and that remains ungapped below 10 K [20]. With a further decrease in temperature, $ZrTe_3$ exhibits filamentary SC below 2 K with no diamagnetic response in $H = 10$ Oe [27]. The origin of filamentary SC is still unclear, and it can be suppressed with $P \sim 0.8$ GPa [28]. Cu has been intercalated in $ZrTe_3$ with $x = 1.9$ in Cu_xZrTe_3, though no SC was discovered [29].

In this Letter, we report the coexistence of CDW and bulk SC in Cu_xZrTe_3, grown via chemical vapor transport. The Cu content x varied within the batch, and the results shown here are on crystals with optimum T_c for $x \approx 0.05$.

Single crystals of Cu_xZrTe_3 ($x = 0$, 0.05) with a typical size of $1 \times 3 \times 0.06$ mm^3 elongated along the $\hat{b}$ axis were grown from pure elements in a mole ratio of Cu:Zr:Te = (0, 0.1):1:3 with 5 mg cm^{-3} iodine sealed in an evacuated quartz tube. The furnace gradient was kept between 1023 and 923 K after heating at 973 K for two days. Elemental analysis was performed by using energy-dispersive x-ray spectroscopy in a JEOL JSM-6500 scanning electron microscope. Resistivity and magnetization were measured in Quantum Design PPMS-9 and MPMS-XL-5, respectively. The observed (Cu $K\alpha$ radiation of Rigaku Miniflex) and calculated [30] (Rietica software) powder x-ray diffraction (XRD) patterns for $ZrTe_3$ and $Cu_{0.05}ZrTe_3$ are shown in Figs. 1(b) and 1(c), respectively. Both can be indexed to $ZrTe_3$. The unit cell refinement yields lattice parameters $a = 0.586(3)$ nm, $b = 0.392(7)$ nm, $c = 1.009(5)$ nm, and $\beta = 97.75(1)°$ for $ZrTe_3$, whereas for $Cu_{0.05}ZrTe_3$ we obtained $a = 0.588(2)$ nm, $b = 0.392(8)$ nm, $c = 1.011(1)$ nm, and $\beta = 97.75(1)°$. The Cu intercalation leads to a slight expansion of the $\hat{a}$- and $\hat{c}$-axis parameters. It should be noted that Zr-Zr distances along the $\hat{b}$-axis chains are unchanged [16].

We observe the onset of SC at $T = 3.8$ K in $\hat{b}$-axis resistivity ρ_b [Fig. 2(a)]. The transition width (10%–90%) is 0.28 K. Figures 2(b) and 2(c) show magnetic properties of $Cu_{0.05}ZrTe_3$ in the superconducting state. The shape of the magnetic hysteresis loop [Fig. 2(b)] is typical of type-2 inhomogeneous superconductors with some electromagnetic granularity. This is in agreement with the transition from the real part of ac susceptibility (χ'_{ac}) curve [Fig. 2(c)], and is similar to data in $SmFeAsO_{0.85}F_{0.15}$ [31]. The χ'_{ac} becomes diamagnetic around $T = (4.0 \pm 0.2)$ K [Fig. 2(c)], confirming SC. The χ'_{ac} decreases gradually with the decrease in temperature, showing no sign of saturation down to 1.8 K. The large estimated superconducting volume fraction at $T = 1.8$ K ($4\pi\chi'_{ac} \sim 94\%$) reveals the bulk nature of SC in $Cu_{0.05}ZrTe_3$, as opposed to the pure material [27].

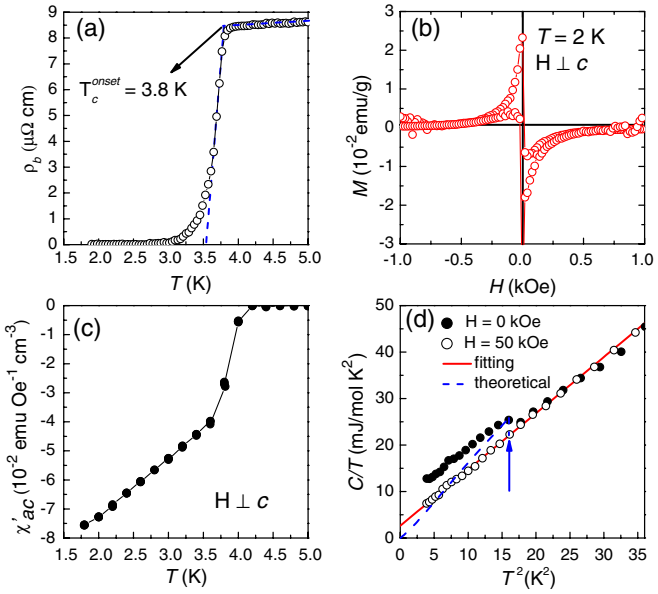

FIG. 2 (color online). (a) $\rho_b(T)$ of $Cu_{0.05}ZrTe_3$ near T_c. (b) The magnetic hysteresis loop measured at $T = 2$ K for $H \perp c$. (c) The temperature dependence of the real part of χ_{ac}. (d) (C/T) of $Cu_{0.05}ZrTe_3$ as a function of T_2 for $H = 0$ (solid circles) and $H \| c = 50$ kOe (open circles). The solid line represents the fitting of the C/T vs T^2 curve for $H \| c = 50$ kOe. The dashed line represents the theoretical curve (see text). The arrow marks the specific heat jump.

Figure 2(d) depicts the specific heat divided by T (C/T) as a function of T^2 of $Cu_{0.05}ZrTe_3$ in $H = 0$ kOe and $H \| c = 50$ kOe. Superconducting transition is suppressed in 50 kOe and from the linear fit $C/T = \gamma + \beta T^2$ we obtain $\gamma = 2.64 \pm 0.12$ mJ/mol K^2 and $\beta = 1.21 \pm 0.01$ mJ/mol K^4. A Debye temperature $\Theta_D = 186(1)$ K can be estimated using $\Theta_D = [\frac{1.944 \times 10^6 \times N}{\beta}]^{1/3}$ where N is the number of atoms per formula unit. From the McMillan formula [32]

$$\lambda = \frac{\mu^* \ln(\frac{1.45T_C}{\Theta_D}) - 1.04}{1.04 + \ln(\frac{1.45T_C}{\Theta_D})(1 - 0.62\mu^*)}, \quad (1)$$

we estimate the electron–phonon coupling constant $\lambda \sim 0.68$ by assuming $\mu^* = 0.13$ for the Coulomb pseudopotential. This is a typical value of an intermediate coupled BCS superconductor. A specific heat jump $(\Delta C/\gamma T_c)$ around $T = 4$ K [Fig. 2(d)] confirms bulk SC. The dashed curve depicted in Fig. 2(d) is the calculated result of the isotropic BCS gap with $2\Delta/k_BT_c = 3.53$ and $\Delta C/\gamma T_c = 1.43$. The C/T vs T^2 curve of $Cu_{0.05}ZrTe_3$ does not follow the calculated result in the superconducting state, most likely due to the sample inhomogeneity. Yet, a $\Delta C/\gamma T_c$ larger than 1.43 can be estimated from the Fig. 2(d), suggesting the intermediate or strong phonon-electron coupling.

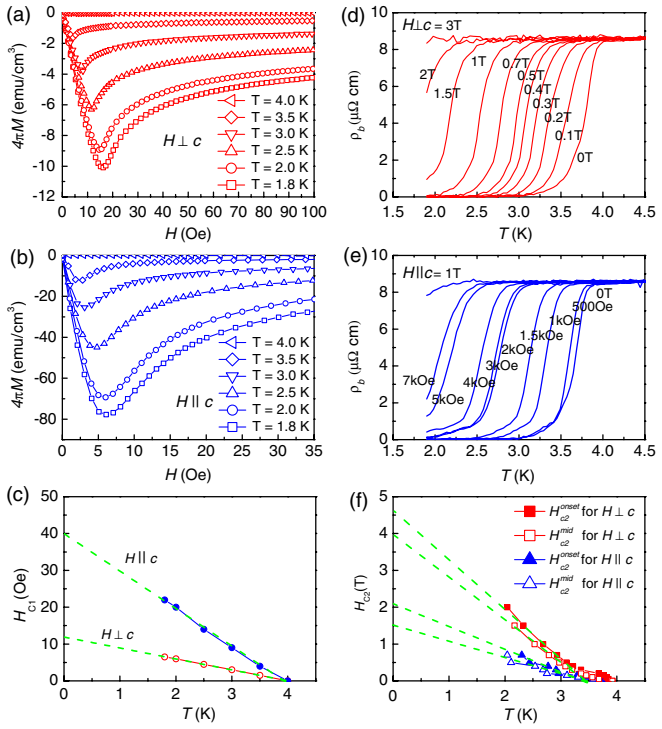

FIG. 3 (color online). (a) Field dependence of magnetization of $Cu_{0.05}ZrTe_3$ for $H \perp c$. (b) Field dependence of magnetization of $Cu_{0.05}ZrTe_3$ for $H \| c$. (c) Temperature dependence of H_{c1} for $H \perp c$ and $H \| c$. The dashed lines are the fitted lines. (d) $\rho_b(T)$ of $Cu_{0.05}ZrTe_3$ for $H \perp c$. (e) $\rho_b(T)$ of $Cu_{0.05}ZrTe_3$ for $H \| c$. (f) $H_{c2}(T)$ onset and $H_{c2}(T)$ midpoint (see text) of $Cu_{0.05}ZrTe_3$.

Figures 3(a) and 3(b) show field dependence of magnetization of $Cu_{0.05}ZrTe_3$ measured at different temperatures for $H \perp c$ and $H \| c$. For $H \| c$, the H_{c1} is obtained using the demagnetization correction [33]. The $H_{c1}(T)$ shows almost linear rather than $H_{c1} = H_{c1}(0)[1 - (T/T_c)^2]$ temperature dependence for both field orientations [Fig. 3(c), dashed lines]. Thus, we estimate $H_{c1}(0) = -0.693 \frac{\partial H_{c1}}{\partial T} T|_{T=T_c}$ from the Werthamer-Helfand-Hohenberg (WHH) equation [34] and we obtain 8.3 (1) Oe ($H \perp c$) and 27.7(4) Oe ($H \| c$).

Figures 3(d) and 3(e) show anisotropic $\rho_b(T)$ of $Cu_{0.05}ZrTe_3$ measured in different fields. Figure 3(f) plots the temperature dependence of H_{c2}^{onset} (onset) and H_{c2}^{mid} (midpoint, 50% of ρ in the normal state). $H_{c2}(0)$ are estimated from the linear H_{c2}-T relation with WHH equation. Because of small variance in the in-plane resistivity values [17], we assume that coherence lengths are isotropic in the $\hat{a}$-$\hat{b}$ plane ($\xi_a \sim \xi_b = \xi_{ab}$) and we estimate [35] coherence lengths using $H_{c2}^c(0) = \Phi_0/(2\pi\xi_{ab}^2)$ and $H_{c2}^{ab}(0) = \Phi_0/(2\pi\xi_{ab}\xi_c)$ where Φ_0 is the flux quantum. The Ginzburg—Landau (GL) parameters κ_i and penetration depths are estimated from $H_{c2}^i(0)/H_{c1}^i(0) = 2\kappa_i^2/\ln\kappa_i$ ($i = ab,\ c$) and $\kappa_{ab}(0) = \lambda_{ab}(0)/\xi_c(0)$, respectively. Finally, from $H_c(0) = H_{c1}^{ab}(0)/\sqrt{2}\kappa_{ab}(0)$, we estimate the thermodynamic critical field. The anisotropy in obtained superconducting parameters can be approximately estimated from the anisotropic GL relation

$$\gamma_{\text{anis}} = \sqrt{\Gamma} = \frac{H_{c2}^{ab}}{H_{c2}^{c}} = \frac{\xi_{ab}}{\xi_c} = \frac{\lambda_c}{\lambda_{ab}} = \frac{\kappa_{ab}}{\kappa_c} \sim \frac{H_{c1}^{c}}{H_{c1}^{ab}}, \qquad (2)$$

where $\Gamma = \frac{m_c^*}{m_{ab}^*} = \frac{\rho_c}{\rho_{ab}}$ with the effective electron mass m_i^* along the i direction. The obtained mass tensor anisotropy $\Gamma \sim 7$ is comparable with the experimental resistivity ratio $\sim$10 of $ZrTe_3$ [16]. This points to small anisotropy in the gap function $\Delta(k_F)$ [36]. We list the obtained superconducting parameters in Table I.

The CDW and SC in $ZrTe_3$ exhibit a rich interplay at high pressures [28]. The T_{CDW} initially increases below 2 GPa and then decreases up to the vanishing point T_{CDW} $\sim$40 K at 5 GPa. Coincidently, a reentrant SC phase emerges at that P and its T_c rises above 4 K up to 11 GPa. In intercalated crystals $Cu_{0.05}ZrTe_3$, only a weak anomaly at T_{CDW} in $\rho_a(T)$-ρ_0 (where ρ_0 is the residual resistivity) can be observed [Fig. 4(a)], whereas the Cu intercalation has no effect on $\rho_b(T)$-ρ_0 [Fig. 4(b)]. This is in contrast to the observed shift of the resistivity hump anomaly for $ZrTe_3$ [$\rho_a(T)$] with $0 < P < 5$ GPa [28] and 1T-$TiSe_2$ [3,13]. The weaker resistivity anomaly around CDW transition in $Cu_{0.05}ZrTe_3$ reflects a smaller reduction of density of states at the Fermi surface [28], but enhanced ρ_0 for $\rho_a(T)$ in $Cu_{0.05}ZrTe_3$ implies more defect scattering. This suggests that the CDW energy gap of Fermi surface is partially filled. Anisotropic lattice expansion via Cu intercalation is rather different from the isotropic high pressures.

Even though the absolute values of resistivity are quasi-two-dimensional [17], we show evidence for inherent in-plane anisotropy. The scattering along the $\hat{b}$ axis in the intercalated and the pure material is not related to the CDW. In quasi-one-dimensional chains, the electron–electron umklapp process will result in a

TABLE I. Parameters of superconducting state in $Cu_{0.05}ZrTe_3$.

$Cu_{0.05}ZrTe_3$		$H_{c2}^i(0)$ (kOe)	$H_{c1}^i(0)$ (Oe)	$H_c(0)$ (Oe)	$\kappa_i(0)$	$\xi_i(0)$ (nm)	$\lambda_i(0)$ (nm)
$i = ab$	Onset	32(4)	8.3(1)	240(30)	93(14)	16(1.2)	605(210)
	Mid	27(3)		225(27)	85(11)	18(1.8)	570(184)
$i = c$	Onset	13(2)	27.7(4)	330(50)	28(5)	6.5(1.3)	1490(420)
	Mid	10(2)		295(50)	24(5)	6.7(1.3)	1539(477)

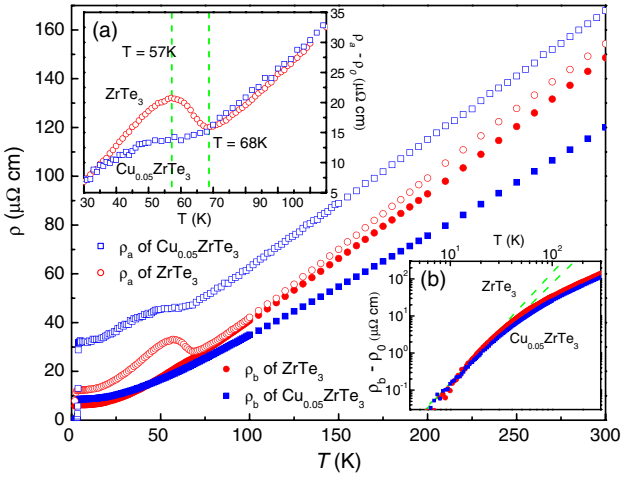

FIG. 4 (color online). Temperature dependence of resistivity along Zr-Zr chains (ρ_b) and orthogonal to the chains (ρ_a) for $ZrTe_3$ and $Cu_{0.05}ZrTe_3$. (a) Temperature dependence of ρ_a-ρ_0 for $ZrTe_3$ and $Cu_{0.05}ZrTe_3$; the peak ($T = 57$ K) and the valley ($T = 68$ K) of CDW anomaly in $ZrTe_3$ are marked with two dashed green lines. (b) Logarithmic plots of temperature dependence for ρ_b-ρ_0 with fitting results (dashed green lines) for the umklapp scattering process (see text).

$\rho(T) = \rho_0 + AT^n$ (where $2 \leq n \leq 3$) for $k_BT < (0.1\text{–}0.3)|\delta|$, and in a linear relation at high temperature for $k_BT > |\delta|$ [37]. The parameter A is a constant and the $|\delta|$ is the typical interchain interaction energy. The $\rho_b(T)$-ρ_0 along Zr-Zr metal in both intercalated and pure material follow this theory very well. The power law temperature dependence is observed for $T < 25$ K with $n = 2.98 \pm 0.03$ and $n = 2.70 \pm 0.03$ for $ZrTe_3$ and $Cu_{0.05}ZrTe_3$, respectively [Fig. 4, inset (b)]. The estimated $|\delta|$ range is (100–250) K, which is consistent with the observed linear $\rho_b(T)$ above 180 K (Fig. 4).

In summary, we have shown that Cu intercalation in $ZrTe_3$ results in the expansion of the lattice parameters in the $\hat{a}$-$\hat{c}$ direction and partial filling of the CDW energy gap. Bulk SC with $T_c = 3.8$ K is discovered in $Cu_{0.05}ZrTe_3$, and its superconducting parameters are given. The electron–electron umklapp scattering is the dominant scattering mechanism along $\hat{b}$ axis. More measurements at higher P and different Cu intercalation x are needed in order to confirm the existence of the $T_c(P, x)$ dome in Cu_xZrTe_3. Further spectroscopic studies would be of interest in order to unfold the details of the phonon mode softening and CDW melting as a function of Cu intercalation.

We thank John Warren for the help with SEM measurements. This work was carried out at BNL, which is operated for the U.S. Department of Energy by Brookhaven Science Associates DE-Ac02-98CH10886.

*Present address: High Magnetic Field Laboratory, Chinese Academy of Sciences, Hefei 230031, People's Republic of China.

[1] R. E. Peierls, Ann. Phys. (Leipzig) **396**, 121 (1930).
[2] G. Gruner, *Density Waves in Solids* (Addison-Wesley, Reading MA, 1994).
[3] E. Morosan *et al.*, Nature Phys. **2**, 544 (2006).
[4] Qimiao Si and Frank Steglich, Science **329**, 1161 (2010).
[5] P. Gegenwart *et al.*, Nature Phys. **4**, 186 (2008).
[6] S. E. Sebastian *et al.*, Proc. Natl. Acad. Sci. U.S.A. **107**, 6175 (2010).
[7] P. Monthoux *et al.*, Nature (London) **450**, 1177 (2007).
[8] D. J. Scalapino, Science **284**, 1282 (1999).
[9] H. Barath *et al.*, Phys. Rev. Lett. **100**, 106402 (2008).
[10] K. Sun *et al.*, Phys. Rev. B **78**, 085124 (2008).
[11] J. F. Zhao *et al.*, Phys. Rev. Lett. **99**, 146401 (2007).
[12] S. Y. Li *et al.*, Phys. Rev. Lett. **99**, 107001 (2007).
[13] A. F. Kusmartseva *et al.*, Phys. Rev. Lett. **103**, 236401 (2009).
[14] S. Hellmann *et al.*, Phys. Rev. Lett. **105**, 187401 (2010).
[15] P. Monceau *et al.*, Phys. Rev. Lett. **39**, 161 (1977).
[16] K. Stöwe and F. R. Wagner, J. Solid State Chem. **138**, 160 (1998).
[17] S. Takahashi *et al.*, Solid State Commun. **49**, 1031 (1984).
[18] D. J. Eaglesham *et al.*, J. Phys. C **17**, L697 (1984).
[19] M. Hoesch *et al.*, Phys. Rev. Lett. **102**, 086402 (2009).
[20] A. Perucchi *et al.*, Eur. Phys. J. B **48**, 489 (2006).
[21] T. Yokoya *et al.*, Phys. Rev. B **71**, 140504 (2005).
[22] M. Hoesch *et al.*, Phys. Rev. B **80**, 075423 (2009).
[23] J. Ishioka *et al.*, Phys. Rev. Lett. **105**, 176401 (2010).
[24] R. Z. Bachrach *et al.*, Phys. Rev. Lett. **37**, 40 (1976).
[25] T. E. Kidd *et al.*, Phys. Rev. Lett. **88**, 226402 (2002).
[26] G. Li *et al.*, Phys. Rev. Lett. **99**, 167002 (2007).
[27] H. Nakajima *et al.*, Physica (Amsterdam) **143B+C**, 240 (1986).
[28] R. Yomo *et al.*, Phys. Rev. B **71**, 132508 (2005).
[29] W. Finckh *et al.*, J. Alloys Compd. **262–263**, 97 (1997).
[30] B. Hunter, Int. Un. Cryst. Comm. Newsletter **20**, 21 (1998).
[31] C. Senatore *et al.*, Phys. Rev. B **78**, 054514 (2008).
[32] W. L. McMillan, Phys. Rev. **167**, 331 (1968).
[33] X. D. Zhu *et al.*, J. Phys. Condens. Matter **21**, 145701 (2009).
[34] N. R. Werthamer *et al.*, Phys. Rev. **147**, 295 (1966).
[35] J. R. Clem, Physica (Amsterdam) **162C–164C**, 1137 (1989).
[36] P. Miranovic *et al.*, J. Phys. Soc. Jpn. **72**, 221 (2003).
[37] A. Oshiyama *et al.*, J. Phys. Soc. Jpn. **45**, 1136 (1978).